SEA ICE MOTION ESTIMATION IN THE MARGINAL ICE ZONE USING DUAL-POLARIZATION SAR

Thomas Kræmer, Camilla Brekke, and Torbjørn Eltoft

University of Tromsø, 9037 Tromsø, Norway, Email: thomas.kramer@uit.no

ABSTRACT

This paper discusses problems found when applying current techniques for estimating sea ice motion using synthetic aperture radar (SAR) to a non-trivial dataset covering the Barents Sea. We review two commonly used similarity measures and their weaknesses when the ice rotates and deforms. We then extend a current algorithm to include rotation estimation and give some considerations on parameter selection. Initial impressions from the use of HV polarization to complement use of HH polarization is also discussed.

Key words: Sea ice; Motion estimation; Synthetic Aperture Radar.

1. INTRODUCTION

The importance of accurate estimates of sea ice motion is widely recognized because of its role in tactical navigation, polar oceanography and global climate research [6, 4]. On the one hand, increasing activity in the Arctic introduces a need for high resolution estimates of ice type and motion in both time and space. On the other hand, climate studies require wide coverage and long timeseries in order to make inferences on large scale trends.

Synthetic aperture radar (SAR) has become an important sensor for remote sensing of sea ice due to its all-weather, day and night imaging capabilities. The high revisit times and large spatial coverage of spaceborne SAR systems will continue to be improved to allow continuous monitoring of sea ice over large areas.

Sea ice motion estimation remains a difficult problem because the ice is moving and deforming rapidly. From one scene to another, the appearance of the ice may change, not only due to the physical changes of the ice and its interaction with the radar signal, but also because of differences in the satellite imaging geometry. Estimation is further complicated by the noise-like phenomenon known as speckle, inherent in any coherent imaging technique.

Algorithms for estimating sea ice motion from spaceborne SAR have been operational for 20 years now [5]. While existing algorithms estimate motion well in regions of dense pack ice, motion estimation in the marginal ice zone (MIZ) where large deformation occurs is still an open area of research.

The objective of this work is to extend the algorithm from Thomas et al. [8] by including rotation estimation. We also report initial impressions on the use of dual-polarization SAR in sea ice tracking.

2. BACKGROUND

Most algorithms for estimating sea ice motion detect the displacement $\mathbf{d} = (d_x, d_y)$ that maximizes some similarity measure $\phi(\mathbf{d})$ between image patches on a regular grid:

$$\mathbf{d} = \arg \max_{(d_x, d_y)} \phi(\mathbf{d}) \tag{1}$$

The choice of similarity measure directly influences the types of motions that can be estimated (see Sec. 3). Correlation based similarity measures track image patches under the assumption that the appearance of the ice does not change significantly between acquisitions. This assumption is reasonable as long as the motion is predominantly translational and densly sampled in time, but does not hold in regions where the ice undergoes strong deformation and rotation [2, 4].

Previous studies on sea ice motion tracking has focused mainly on the use of single channel copolarization SAR data. Recently there have been indications that the use of multi-polarization data may be beneficial [2, 3]. With new satellites and constellation missions, multi-polarization data with high temporal resolution are readily available which may provide additional information in areas that are difficult to track (e.g. highly homogeneous areas).

3. METHODOLOGY

The basis for our work is presented in Thomas et al. [8], which we have modified to include rotation estimation (see Sec. 3.2). The algorithm is a cascaded pyramid motion tracking algorithm where displacement estimates at a coarse resolution is used as initial estimates for the next resolution level.

The following section discusses common similarity measures used in such tracking schemes and their weaknesses. We then discuss the use of the log-polar transform (LPT) to better account for rotational motion.

3.1. Similarity measures for motion tracking

The most common similarity measure between two image patches $f(\mathbf{x})$ and $g(\mathbf{x})$ of equal sizes with mean intensities μ_f and μ_g is the *normalized cross-correlation* (NCC)

$$\rho_{fg}(\mathbf{d}) = \frac{\sum_i [f(\mathbf{x}_i) - \mu_f][g(\mathbf{x}_i) - \mu_g]}{\sqrt{\sum_i [f(\mathbf{x}_i) - \mu_f]^2} \sqrt{\sum_i [g(\mathbf{x}_i) - \mu_g]^2}} \quad (2)$$

where the sum is over all pixels in each patch. The NCC has the advantage of being illumination invariant [1, 8].

Because of the high computational cost of computing the NCC, correlation in the Fourier domain is often used to detect a set of candidate displacements, from which the best match is determined using NCC [7]. Let $F(\mathbf{u}) = \mathcal{F}\{f(\mathbf{x})\}$ and $G(\mathbf{u}) = \mathcal{F}\{g(\mathbf{x})\}$ where $\mathcal{F}\{\cdot\}$ denotes the Fourier transform and $\mathbf{u} = (u, v)$ denote the spatial frequencies in the x- and y-direction. The *phase correlation* (PC) similarity measure is computed by inverting the normalized cross-power spectrum of the two image patches:

$$\zeta_{fg}(\mathbf{d}) = \mathcal{F}^{-1}\left\{\frac{F(\mathbf{u})G^*(\mathbf{u})}{|F(\mathbf{u})G^*(\mathbf{u})|}\right\} \quad (3)$$

The underlying assumption when using NCC and PC for motion estimation is that motion is translational. In the MIZ this assumption is rarely valid. The NCC compares image patches by direct comparison between pixels. Naturally this will be unreliable when structures in one patch has been subject to rotation and deformation.

If rotation of the ice occurs at a scale much larger than the analysis window, NCC can usually be used sucessfully, but for rotations at the size or smaller than the analysis window, NCC and PC scores will be low even at the correct position. We therefore introduce rotation estimation into the framework proposed by Thomas et al. [8] to obtain better NCC values in deformation zones.

3.2. Log-polar transformation

If the assumption of translational motion is relaxed to an affine motion expressing a rigid transformation without scaling or shear, we get a three parameter model where two translation parameters and a rotation angle need to be estimated. Rotation and scaling of an image results in rotation and scaling of its magnitude spectrum. By converting the magnitude spectrum to a polar coordinate system,

$$r = \sqrt{(u - u_c)^2 + (v - v_c)^2} \quad (4)$$

$$\theta = \tan^{-1}\left(\frac{v - v_c}{u - u_c}\right) \quad (5)$$

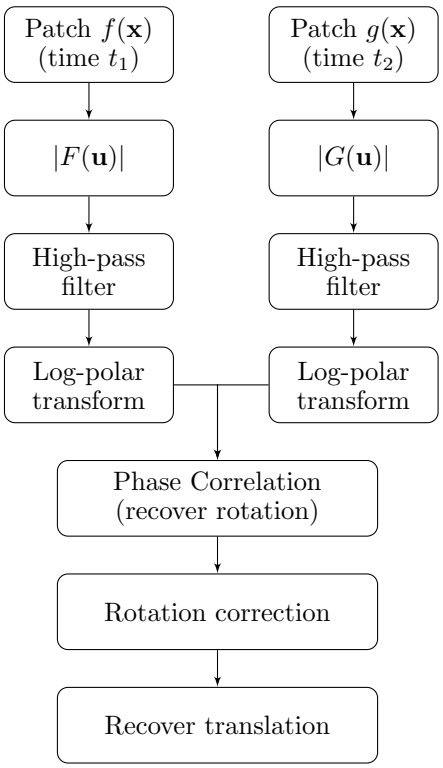

Figure 1: Rotation is estimated from the cross-power spectrum of the log-polar transformed magnitude spectrum of each image. Translation is subsequently estimated from the cross-power spectrum of the template image and the rotation-corrected target image.

a rotated magnitude spectrum is converted to a translated spectrum in polar coordinates. (u_c, v_c) is the origin of the magnitude spectrum. This allows us to estimate the rotation by PC in the transformed domain. If the r-axis is made logarithmic, scale changes will also be transformed to translations in the $(\log r, \theta)$-coordinates of the log-polar transform domain. In principle, both scale and rotation can be recovered from the LPT, but only rotation has been considered at this point.

Because of the computational burden introduced by the additional Fourier transforms, rotation estimation should only be performed if there is an indication that rotation may have occurred. Therefore, the NCC value is considered to be reliable as long as the score is higher than a specified threshold T. In the event that $\rho \leq T$, rotation estimation is invoked and the NCC after rotation correction (ρ_r) is compared to the NCC before correction (ρ). If $\rho_r > \rho$ and $\rho_r > T$, then the estimate is accepted. The procedure for rotation estimation is shown in Fig. 1. Fig. 2 shows an example of the magnitude spectrum and corresponding LPT for two image patches.

3.3. Parameter selection

The algorithm by Thomas et al. [8] requires the specification of the number of pyramid levels, an initial search window size and the number of cascades. Image dimensions and window sizes are assumed to be

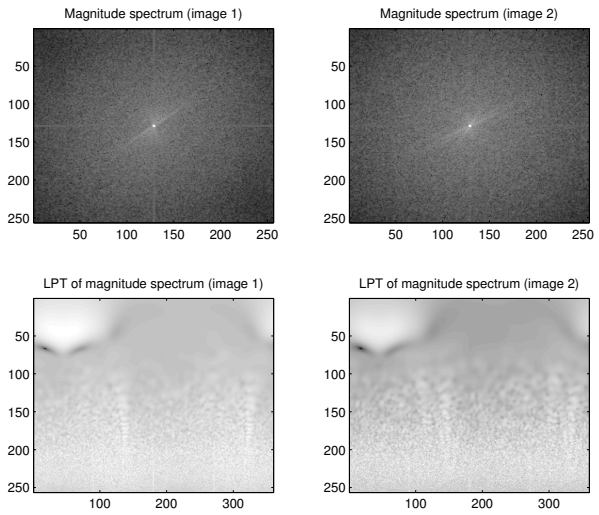

Figure 2: Log-polar transformation of the magnitude spectra of two images. Rotation is estimated from the cross-power spectrum of the bottom two images.

powers of two. The size of the search window is goverened by the requirement that the same pattern must be visible in both image patches. This involves a trade-off. A large window size will contain many samples, but we risk including multiple motions in the window.

The initial search window size ω_L used at the coarsest pyramid level L needs to be at least twice as large as the expected ice displacement in pixels $d_{\max}$ (which can be calculated from the maximum expected ice speed in the region, the time difference between images and the nominal pixel resolution):

$$\omega_L = 2^{\lceil \log_2(2 * d_{\max}/N_L) \rceil} \tag{6}$$

The number of pyramid levels N_L is chosen manually such that distinct ice structures (e.g. pressure ridges) are still visible. At each cascade, the window size is reduced to half the size of the previous cascade.

For highly homogeneous image regions there is insufficient information to reliably estimate motion. Therefore, instead of specifying the number of cascades we stop at a specified estimation resolution ω_0 (e.g. when motion has been estimated with a search window of size $\omega_0 = 8$). The number of cascades N_c is calculated as

$$N_c = \log_2(\omega_L) - \log_2(\omega_0). \tag{7}$$

Ideally estimation should adapt to the data and stop when there is insufficient information to get a reliable match.

4. DATA

Our dataset consists of 40 dual-polarized RadarSat-2 ScanSAR Wide scenes acquired in 1–4 day intervals from April 6 to July 15, 2010 over the Barents Sea, East of Svalbard. During the period of acquisition, six buoys were deployed in the area, five on drifting ice floes and one on an iceberg.

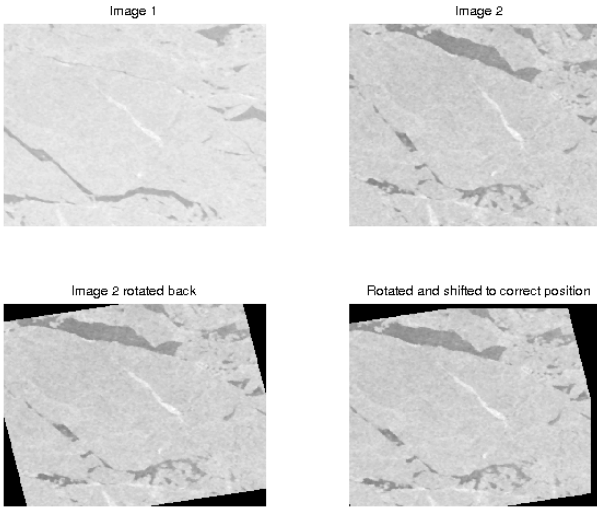

Figure 3: Image 2 rotated and translated to better match Image 1.

5. EXPERIMENTAL RESULTS

5.1. Rotation

Fig. 3 shows the result of correcting the rotation and translation estimated with PC in the LPT domain. Even though this is a mild rotation, NCC values increased from ~ 0.2 to ~ 0.6. The reason for introducing the LPT was that the algorithm observed low correlation values in regions where the position was accurate, meaning that the NCC values were misleading. Introducing rotation estimation into the algorithm improved correlation scores in regions where rotation could be estimated reliably.

Running a high-pass filter on speckled data is not without risk. It is important to apply a speckle-filter to the images before the rotation module. A simple box-median filter was enough for our dataset (RS2 ScanSAR Wide data are already multilooked at delivery), but this may not be sufficient for more speckled data. Rotation estimation using this method only makes sense if there are distinct patterns which allow unambiguous estimates. Therefore, the conditional rotation estimation is only estimated at the first few cascades, before switching to using NCC.

Using a scheme that assumes a rigid transformation of an image may not be the best choice for tracking the sea ice medium. Large floes may move with a rigid body motion, but ice in general are subject to complex deformation which suggest that a tracking algorithm that allows for non-rigid transformations may be better suited for tracking sea ice.

5.2. Polarization

That HV-polarization is better for ice/ocean discrimination is well-known. We wanted to investigate if use of the HV-polarization could be used to complement use of HH-polarization for sea ice tracking.

The images in our dataset were acquired during the melting season, which has an impact on the received radar signal. The HV signal is much weaker than the HH signal for the whole time series.

Running our algorithm on HH and HV polarizations separately produced very similar results for regions with distinct patterns. The HH and HV channels were very similar. If water is masked out the correlation coefficient between HH and HV channels was typically in the order of 0.95. Studying regions of low correlation between the channels indicated that the HV-channel appeared more homogeneous than the HH-channel. Also, the further into the melting season, the more featureless the ice signature in the HV channel seems to get. Use of cross-polarization may therefore only be useful for winter images.

5.3. Validation with buoys

The motion estimates derived from the images are validated using a set of six GPS tracks from deployed buoys with good results. Unfortunately, there were no buoys in the areas of interest where the algorithms perform poorly. Therefore, the usefulness of the buoy information as independent measurements is limited to investigating the accuracy in regions where the existing algorithms should work well. Fig. 4 shows that buoy tracks and estimated tracks are in good agreement. We are currently working on comparing tracking results in the MIZ with manually drawn vectors to quantify its performance in more severe deformation zones.

6. CONCLUSIONS AND FUTURE WORK

We have extended a current algorithm for sea ice tracking by including rotation estimation through the LPT which improved registration accuracy where rotation could be reliably estimated.

Our impression is that for the melting season, HH-polarization is still preferable to HV-polarization.

Future work includes investigating other similarity measures for tracking non-rigid motion. We also want to be able to set parameters like the number of pyramid levels and the number of cascade steps automatically, based on the data. This involves quantifying the distinctness of patterns in the image.

ACKNOWLEDGEMENTS

This work was funded by the research council of Norway through the Arctic Earth Observation and Surveillance Technologies project. The data were acquired from MarinTek, the University Centre in Svalbard and Kongsberg Satellite Services through the MarSafe project. RADARSAT-2 Data and Products ©MacDONALD, DETTWILER AND ASSOCIATES LTD. (2011) All Rights Reserved.

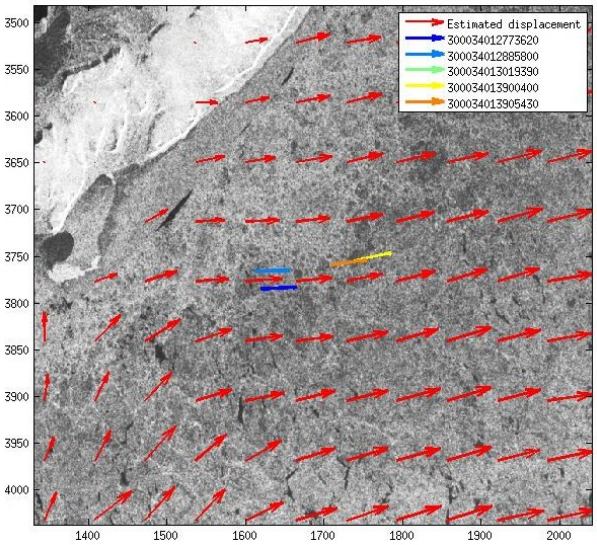

Figure 4: Displacement estimates compared with GPS positions showing good agreement.

RADARSAT is an official mark of the Canadian Space Agency.

REFERENCES

[1] Fily, M. and Rothrock, D. A. (1986). Extracting sea ice data from satellite SAR imagery. *IEEE Transactions on Geoscience and Remote Sensing*, GE-24(6):849–854.

[2] Hollands, T. and Dierking, W. (2011). Performance of a multiscale correlation algorithm for the estimation of sea-ice drift from SAR images: initial results. *Annals of Glaciology*, 52(57):311–317.

[3] Komarov, A. and Barber, D. (2012). Detection of sea ice motion from co- and cross-polarization RadarSat-2 images. In *Proc. IGARSS*, volume 7, pages 3277–3280.

[4] Kwok, R. (2010). Satellite remote sensing of sea-ice thickness and kinematics: a review. *Journal of Glaciology*, 56(200):1129–1140.

[5] Kwok, R. and Pang, A. (1992). Performance of the ice motion tracker at the Alascka SAR facility. In *IGARSS*, pages 26–29.

[6] Leppäranta, M. (2005). *The drift of sea ice*. Springer.

[7] Thomas, M. V., Geiger, C., and Kambhamettu, C. (2008). High resolution (400 m) motion characterization of sea ice using ERS-1 SAR imagery. *Cold Regions Science and Technology*, 52(2):207–223.

[8] Thomas, M. V., Kambhamettu, C., and Geiger, C. A. (2011). Motion tracking of discontinuous sea ice. *IEEE Transactions on Geoscience and Remote Sensing*, 49(12):5064–5079.